[Article] www.whxb.pku.edu.cn

# $BaTiO_3$的电子结构和光学性质

张子英[1] 杨德林[2,*] 刘云虎[1] 曹海滨[1] 邵建新[1] 井 群[1]
([1]石河子大学师范学院物理系, 生态物理重点实验室, 新疆 石河子 832003; [2]郑州大学物理工程学院, 郑州 450052)

**摘要:** 采用第一性原理赝势平面波方法, 在局域密度近似(LDA)和广义梯度近似(GGA)下分别计算了$BaTiO_3$立方相和四方相的电子结构, 并在局域密度近似下计算了$BaTiO_3$立方相的光学性质. 结果表明, $BaTiO_3$立方相和四方相都为间接带隙, 方向分别为$\Gamma$-$M$和$\Gamma$-$X$, 大小分别为2.02和2.20 eV. 对$BaTiO_3$和$PbTiO_3$铁电相短键上电子布居数的对比分析, 给出了它们铁电性大小的差别. 且在30 eV的能量范围内研究了$BaTiO_3$的介电函数、吸收系数、折射系数、湮灭系数、反射系数和能量损失系数等光学性质, 并基于电子能带结构对光学性质进行了解释. 计算结果与实验数据相符合.

**关键词:** 电子结构; 密度泛函理论; 光学性质; 赝势平面波方法
**中图分类号:** O641

# Electronic Structures and Optical Properties of $BaTiO_3$

ZHANG Zi-Ying[1] YANG De-Lin[2,*] LIU Yun-Hu[1] CAO Hai-Bin[1]
SHAO Jian-Xin[1] JING Qun[1]
([1]*Key Laboratory of Ecophysics, Department of Physics, Teachers College, Shihezi University, Shihezi 832003, The Xinjiang Uygur Autonomous Region, P. R. China*; [2]*Physics Engineering College, Zhengzhou University, Zhengzhou 450052, P. R. China*)

**Abstract:** The pseudo-potential plane wave (PP-PW) method, the local density approximation (LDA) and generalized gradient approximation (GGA) were used to calculate the electronic structures of cubic and tetragonal $BaTiO_3$, respectively. The local density approximation was used to calculate optical properties of cubic $BaTiO_3$. Results show an indirect bandgap of 2.02 eV in the $\Gamma$-$M$ direction for the cubic phase and an indirect bandgap of 2.20 eV in the $\Gamma$-$X$ direction for the tetragonal phase. For ferroelectric phases, a comparison of shorter bond populations for $BaTiO_3$ and $PbTiO_3$ revealed differences in ferroelectric behavior between $BaTiO_3$ and $PbTiO_3$. Furthermore, the dielectric function, absorption coefficient, refractive index, extinction coefficient, reflectivity, and energy loss coefficient were obtained and analyzed on the basis of electronic band structures for radiation of up to 30 eV. These results are in good agreement with experimental data.

**Key Words:** Electronic structure; Density functional theory; Optical property; Pseudo-potential plane wave method

Barium titanate ($BaTiO_3$) is one of the most important ferroelectric oxides in electronic applications and has a large electro-optic coefficient and a high photorefractive sensitivity, therefore it can be used as an optical sensor[1–3]. $BaTiO_3$ undergoes a succession of phase transitions, from a high-temperature and high-symmetry cubic perovskite phase to a slightly distorted ferroelectric structure with tetragonal, orthorhombic, and rhombohedral symmetry[3]. Several studies have attempted to determine the electronic and optical properties by several first-principles calculation methods[4–12]. Piskunov *et al.*[5] studied the electronic structure of $BaTiO_3$ using the local-density approximation (LDA) and generalized gradient approximation (GGA) together with the linearized augmented plane wave (LAPW) method and found that GGA overestimated the equilibrium volume. Cohen and Krakauer[2]

Received: February 24, 2009; Revised: May 21, 2009; Published on Web: June 23, 2009.
*Corresponding author. Email: Dlyang25@yahoo.cn; Tel: +86-13838113035.
The project was supported by the Natural Science Research and Technology Innovation Program of Shihezi University, China (ZRKX200731).
石河子大学自然科学研究与技术创新(ZRKX200731)资助项目

performed full-potential (FP) LAPW calculations to treat the lattice dynamics and studied the origin of ferroelectricity in $BaTiO_3$. Wample *et al*.[8] studied the dielectric constant, spontaneous polarization, optical absorption, and refractive index for tetragonal $BaTiO_3$ in the energy range between 1.8 and 30 eV. Using the tight-binding linear muffin-tin orbital (TB-LMTO) and the full-potential linear muffin-tin orbital (FP-LMTO) methods, Saha[9] and Ahuja[10] *et al*. discussed the band structures and optical properties of tetragonal $BaTiO_3$ perovskite, respectively. Cai *et al*.[12] studied the optical properties of $BaTiO_3$ with regards to its core-level spectra by first-principles and using the scissor approximation at up to 30 eV. Recently, Kuroiw *et al*.[13] accurately determined charge-density distributions of cubic and tetragonal $PbTiO_3$ and $BaTiO_3$ by a maximum entropy (MEM) analysis. They found that Pb-O hybridization in tetragonal $PbTiO_3$ was more evident than the Ti-O hybridization in tetragonal $BaTiO_3$, and this has been theoretically predicted as a key factor for the far larger ferroelectricity of $PbTiO_3$ compared to $BaTiO_3$. Until now the hybridization of tetragonal $BaTiO_3$ has not been studied theoretically in detail. On the other hand, little theoretical attention has been paid to the difference about the absence of peaks at about 12.32 and 13.32 eV in imaginary part $\varepsilon_2(\omega)$ of the dielectric function $\varepsilon(\omega)$ of $BaTiO_3$ obtained by Cai *et al*.[12] and the absence of peaks in experiment[14]. In this paper, we calculated the electronic structure of $BaTiO_3$ in both cubic and tetragonal phases by using the pseudo-potential plane wave (PP-PW) method with LDA and GGA. In addition, we discussed the difference in ferroelectric behavior between $PbTiO_3$ and $BaTiO_3$ based on calculations of Mulliken charge population of $BaTiO_3$. Furthermore, the optical properties of cubic $BaTiO_3$ at up to 30 eV were studied with the LDA using a dense mesh 20×20×20 grid of Monkhorst-Pack points.

## 1 Method of calculation

First-principles calculations were performed using the Materials Studio 4.1 graphical frontend interface using the Cambridge serial total energy (CASTEP) code[15,16]. The exchange correlation potential within the LDA and GGA was calculated using the Ceperley-Aider and Perdew-Zunger (CA-PZ)[15] and Perdew-Burke-Ernzerh (PBE) schemes[17]. For the CASTEP computer code, the Kohn-Sham equations were solved within the framework of density functional theory[17] by expanding the wave functions of the valence electrons in a basis set of plane waves with a kinetic energy smaller than a specified cut-off energy $E_{cut}$. The presence of tightly-bound core electrons was represented by non-local ultra-soft pseudo-potentials of the Vanderbilt-type[9]. The states of Ba $5s^25p^6 6s^2$, Ti $3d^24s^2$, and O $2s^22p^4$ were treated as valence states. For crystal reciprocal-lattices, integration over the symmetrized Brillouin zone was performed by summing over special *k*-points that were generated from the Monkhorst-Pack scheme[18]. A plane wave cut-off energy of 380 eV and a 6×6×6 grid of Monkhorst-Pack points were employed in this study to ensure good convergence between the computed structures and energies. Structural parameters for $BaTiO_3$ were determined using the Broyden-Fletcher-Goldfarb-Shenno (BFGS) minimization technique with the following thresholds for converged structures, energy change per atom of less than $5\times10^{-6}$ eV, residual force of less than 0.1 eV·nm$^{-1}$, a stress of less than 0.03 GPa, and an atom displacement during the geometry optimization of less than 0.05 pm. Optical properties may be determined using the complex dielectric function $\varepsilon(\omega)=\varepsilon_1(\omega)+i\varepsilon_2(\omega)$. The imaginary part of the dielectric function is given as:

$$\varepsilon_2(\omega)=\frac{Ve^2}{2\hbar m^2\omega^2}\int \mathrm{d}^3k \sum_{nn'}|\langle \vec{k}n|\vec{p}|\vec{k}n'\rangle|^2\times f(\vec{k}n)(1-f(\vec{k}n'))\delta(E_{\vec{k}n}-E_{\vec{k}n'}-\hbar\omega) \quad (1)$$

where $\vec{p}$ is the momentum operator, $e$ is the electronic charge, $V$ is the volume, $\omega$ is the light frequency, $\hbar\omega$ is the energy of the incident phonon, $m$ is electronic mass, $\vec{k}n>$ and $\vec{k}n'>$ are the conduction band (CB) and valence band (VB) wave functions corresponding to the $n$th and $n'$th eigenvalue with crystal momentum $k$, and $f(\vec{k}n)$ is the Fermi distribution function. Evaluation of the matrix elements of the momentum operator in Eq.(1) was done over the muffin-tin and the interstitial regions separately. Further details about the evaluation of matrix elements can be found in Ref.[19]. The real part of the dielectric function can be derived from the imaginary part using the Kramers-Kronig relations.

$$\varepsilon_1(\omega)=1+\frac{2}{\pi}p\int_0^\infty \frac{\varepsilon_2(\omega')\omega'\mathrm{d}\omega'}{\omega'^2-\omega^2} \quad (2)$$

where $p$ is the principal value of the integral. The knowledge of both the real and imaginary parts of the dielectric function allows the calculation of important optical functions. Expressions for the absorption coefficient $I(\omega)$, refractive index $n(\omega)$, extinction coefficient $k(\omega)$, reflectivity $R(\omega)$, and energy-loss coefficient $L(\omega)$ now follow immediately as given below[9,12,20]:

$$I(\omega)=\sqrt{2}(\omega)[\sqrt{\varepsilon_1(\omega)^2+\varepsilon_2(\omega)^2}-\varepsilon_1(\omega)]^{\frac{1}{2}} \quad (3)$$

$$n(\omega)=[\frac{\varepsilon_1(\omega)}{2}+\frac{\sqrt{\varepsilon_1(\omega)^2+\varepsilon_2(\omega)^2}}{2}]^{\frac{1}{2}} \quad (4)$$

$$k(\omega)=\sqrt{\frac{1}{2}}[\sqrt{\varepsilon_1(\omega)^2+\varepsilon_2(\omega)^2}-\varepsilon_1(\omega)]^{\frac{1}{2}} \quad (5)$$

$$R(\omega)=\left|\frac{\sqrt{\varepsilon(\omega)}-1}{\sqrt{\varepsilon(\omega)}+1}\right|^2 \quad (6)$$

$$L(\omega)=\frac{\varepsilon_2(\omega)}{\varepsilon_1(\omega)^2+\varepsilon_2(\omega)^2} \quad (7)$$

The calculation of optical properties usually requires a dense mesh of uniformly distributed *k*-points. We employ Brillouin zone integration with a 20×20×20 grid of Monkhorst-Pack points to the calculation.

## 2 Results and discussion

### 2.1 Structural parameters

X-ray powder diffraction data were used as a starting point for geometry optimization. Cubic $BaTiO_3$ ($a$=0.40 nm) belongs to the space group $O_h^1$[21]. Tetragonal $BaTiO_3$ ($a$=0.3992 nm and $c$=0.4036 nm) belongs to the space group $C_{4v}^1$ and has a small te-

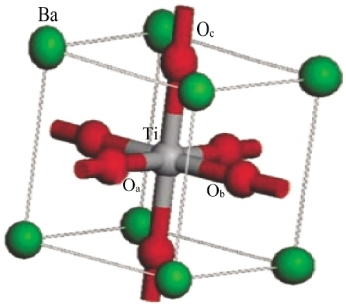


**Fig.1 Structure of the perovskite-type $BaTiO_3$**

**Table 1 $BaTiO_3$ equilibrium lattice constant calculated by various methods**

| Method | Lattice constant (nm) | | | |
|---|---|---|---|---|
| | cubic | tetragonal | | |
| | | *a* | *b* | *c* |
| Expt. | 0.400[22] | 0.3992[23] | 0.3992[23] | 0.4036[23] |
| LCAO(LDA) | 0.396[5] | | | |
| LCAO(GGA) | 0.403[5] | | | |
| FP-LAPW(LAD) | 0.3935[23] | | | |
| PP-PW(LDA) | 0.3943 | 0.394 | 0.394 | 0.395 |
| PP-PW(GGA) | 0.3990 | 0.400 | 0.400 | 0.401 |

tragonal distortion ($c/a$=1.01)[22].

As depicted in Fig.1, both cubic and tetragonal unit cells contain one molecule where atomic positions in the elementary cell are as follows: Ba (0.0, 0.0, 0.0); Ti(0.5, 0.5, 0.5), $O_a$ (0.5, 0.0, 0.5); $O_b$(0.0, 0.5, 0.5); $O_c$ (0.5, 0.5, 0.0). The calculated results for the equilibrium geometry are given in Table1. The experimental data and the previous calculation results[23] are also listed in Table 1 for comparison. By comparison to the experimental lattice parameters, there is a typical underestimate of the LDA, and the GGA approximation gives lattice parameters closer to experimental values. These results are in good agreement with previous calculations[24], but they are slightly different from the values obtained by Piskunov *et al.*[5].

## 2.2 Band structure

Fig.2 and Fig.3 show electronic band structures along the symmetry lines of the Brillouin zone for $BaTiO_3$ in ideal cubic and tetragonal phases, respectively. The energy scale was measured in eV and the top of the valence band (VB) was set to zero on this energy scale. Lower valence bands mainly originate from contributions of O-2*s* and Ba-5*p* orbitals in the region of −20 to −5 eV. There are nine valence bands that are mainly originate from the hybridization of O-2*p* and Ti-3*d* orbitals in the region from −5 to 0 eV (below the Fermi level). These bands are very close and even overlap each other. In the region of the conduction band (CB) (above the Fermi level), there are some bands that originate mainly from the Ti-3*d* or Ba-5*p* orbitals. An indirect band gap of 2.02 eV (without the empirical correction factor) between the top of the VB at point $\Gamma$ and the bottom of the CB at point *M* was observed in the direction ($\Gamma$-*M*), and this is different from the results reported by Saha *et al.*[9] and Ahuja *et al.*[10]. The larger indirect band gap may account for the fact that the peaks of optical spectra in $BaTiO_3$ shift to the higher energy range[25]. Notice that from the band structure of Fig.2, it is not clear whether the band gap is indirect ($\Gamma$-*M*) or direct ($\Gamma$-$\Gamma$), because in both directions the values of band gaps are quite close to each other. An indirect band gap of 2.20 eV (without the empirical correction factor) was observed in the $\Gamma$-*X* direction for the tetragonal phase (Fig.3). By comparison to the cubic phase, the top VB is lower because of hybridization along the polar *c*-direction. These results are consistent with our DOS calculation (Fig.4). The calculated band gap and the values obtained by other methods are summarized in Table 2. The value obtained in our work is smaller than the experimental band gap of about 3.20 eV for the tendency of underestimate of energy-band for

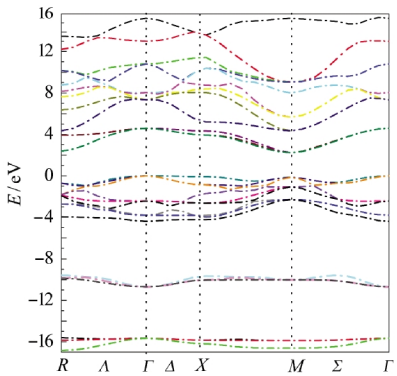


**Fig.2 Band structure of $BaTiO_3$ in cubic phase**

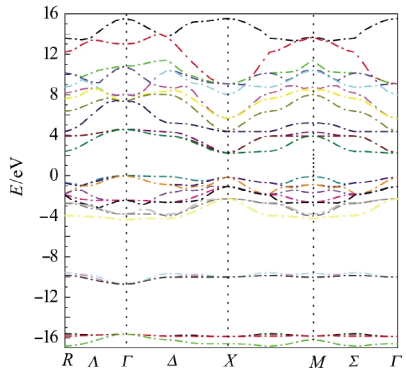


**Fig.3 Band structure of $BaTiO_3$ in tetragonal phase**

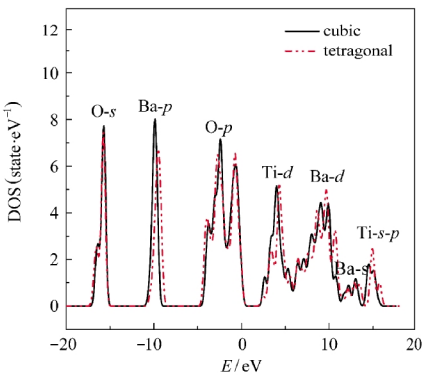


**Fig.4 Total density of states (DOSs) of $BaTiO_3$ in cubic and tetragonal phases**

**Table 2 $BaTiO_3$ band gaps calculated by various methods for cubic and tetragonal phases**

| Method (for cubic) | Band gap (eV) | Direction | Method (for tetragonal) | Band gap (eV) | Direction |
|---|---|---|---|---|---|
| Expt.[8] | 3.20 | $\Gamma$-$\Gamma$ | | | |
| LCAO(LDA)[5] | 1.92 | $R$-$\Gamma$ | FP-LMDO(LDA)[10] | 2.20 | $\Gamma$-$\Gamma$ |
| FP-LMTO (LDA)[9] | 1.2 | $\Gamma$-$\Gamma$ | | | |
| FLAPW-SAT (GGA)[12] | 1.918 | $\Gamma$-$\Gamma$ | | | |
| PP-PW(LDA) | 2.00 | $\Gamma$-$M$ | PP-PW(LDA) | 2.18 | $\Gamma$-$X$ |
| PP-PW(GGA) | 2.02 | $\Gamma$-$M$ | PP-PW(GGA) | 2.20 | $\Gamma$-$X$ |

GGA in solidstate physics, but it is higher than any other theoretically calculated values reported so far.

As a comparison, we also calculated Mulliken charge populations for both cubic and tetragonal $BaTiO_3$ because this helps to understand bonding behavior. Calculated Mulliken charge populations are given in Tables 3 and 4. Charge transfer from Ba and Ti to O is about 1.48$e$ and 1.71$e$, respectively. Bond populations indicate that the degree of electron cloud overlap between two bonding atoms[26]. The highest and the lowest values imply that chemical bonds exhibit covalent or ionic bonding. Positive and negative values indicate bonding and antibonding states, respectively. A value for the overlap population close to zero indicates that there is no significant interaction between the electronic populations of the two atoms. From Table 4, the charge population of $O_c$—Ti decreases slightly with the elongation of the $c$ axis and charge populations of $O_a$—Ti and $O_b$—Ti increase in tetragonal $BaTiO_3$, which indicates hybridization between Ti-3$d$ and O-2$p$ orbitals. This hybridization is responsible for ferroelectricity. Note that charge populations of the shorter O—Ti bonds are small and the O—Ti bonds are ionic in nature for the tetragonal $BaTiO_3$. As a comparison with $PbTiO_3$ in Table 5, the Pb—O bonding nature of the cubic phase was found to be ionic whereas the shorter Pb—O and Ti—O bonds in the tetragonal

**Table 3 Charge of species of $BaTiO_3$**

| Species (cubic) | $Q/e$ | Species (tetragonal) | $Q/e$ |
|---|---|---|---|
| O | −1.06 | O | −1.06 |
| Ti | 1.71 | Ti | 1.71 |
| Ba | 1.48 | Ba | 1.48 |

**Table 4 Mulliken charge population of $BaTiO_3$**

| Bond (cubic) | Charge population ($e$) | Bond length (nm) | Bond (tetragonal) | Chanrge population ($e$) | Bond length (nm) |
|---|---|---|---|---|---|
| $O_a$—Ti | 0.10 | 0.200414 | $O_a$—Ti | 0.12 | 0.200386 |
| $O_b$—Ti | 0.10 | 0.200414 | $O_b$—Ti | 0.12 | 0.200386 |
| $O_c$—Ti | 0.10 | 0.200414 | $O_c$—Ti | 0.07 | 0.200423 |
| $O_a$—Ba | −1.39 | 0.283428 | $O_a$—Ba | −1.39 | 0.283484 |
| $O_b$—Ba | −1.39 | 0.283428 | $O_b$—Ba | −1.39 | 0.283484 |
| $O_c$—Ba | −1.39 | 0.283428 | $O_c$—Ba | −1.39 | 0.283389 |
| $O_a$—$O_b$ | −0.31 | 0.283428 | $O_a$—$O_b$ | −0.31 | 0.283369 |
| $O_a$—$O_c$ | −0.31 | 0.283428 | $O_a$—$O_c$ | −0.31 | 0.283399 |
| $O_b$—$O_c$ | −0.31 | 0.283428 | $O_b$—$O_c$ | −0.31 | 0.283399 |

**Table 5 Mulliken charge population of $PbTiO_3$**

| Bond (cubic) | Charge population ($e$) | Bond length (nm) | Bond (tetragonal) | Charge population ($e$) | Bond length (nm) |
|---|---|---|---|---|---|
| $O_a$—Ti | 0.84 | 0.193368 | $O_a$—Ti | 0.86 | 0.192182 |
| $O_b$—Ti | 0.84 | 0.193368 | $O_b$—Ti | 0.86 | 0.192182 |
| $O_c$—Ti | 0.84 | 0.193368 | $O_c$—Ti | 0.79 | 0.195867 |
| $O_a$—Pb | 0.07 | 0.273463 | $O_a$—Pb | 0.05 | 0.274402 |
| $O_b$—Pb | 0.07 | 0.273463 | $O_b$—Pb | 0.05 | 0.274402 |
| $O_c$—Pb | 0.07 | 0.273463 | $O_c$—Pb | 0.12 | 0.271786 |
| $O_a$—$O_b$ | −0.12 | 0.273463 | $O_a$—$O_b$ | −0.12 | 0.271786 |
| $O_a$—$O_c$ | −0.12 | 0.273463 | $O_a$—$O_c$ | −0.11 | 0.274404 |
| $O_b$—$O_c$ | −0.12 | 0.273463 | $O_b$—$O_c$ | −0.11 | 0.274404 |

phase were covalent because the electron densities of the two corresponding atoms overlapped strongly. These differences are consistent with theoretical predictions[1] and are thus related to the key factor that is responsible for the much larger ferroelectricity of $PbTiO_3$ compared to $BaTiO_3$[13].

### 2.3 Optical properties

Figs.(5−8) show the calculated optical properties at the equilibrium lattice constant and in an energy range from 0 to 30 eV. To account for the structures observed in the optical spectra, it is customary to consider transitions from occupied to unoccupied bands in the electronic energy band structure especially at high symmetry points in the Brillouin zone. Fig.5 shows the calculated dielectric function of $BaTiO_3$. The imaginary part $\varepsilon_2(0)$ of the dielectric function has seven prominent peaks. Peaks A (4.52 eV), B(7.41 eV) , C(8.80 eV), and D(10.28 eV) mainly correspond to the transition from O-2$p$ VB to Ti-3$d$ CB states with a small contribution from Ba 5$p$ states. Peaks E (18.56 eV), F (23.08 eV) and G(24.32 eV) are assigned to the transition of inner electrons from O-2$s$ and Ba-5$p$ levels to the CB. Our result is in good a greement with the result calculated by the FLAPW-SAT method[12] in a low-energy range of less than 10 eV. The absence of peaks at about 12.32 and 13.32 eV in our calculated result is also consistent with experimental data[12]. The calculated static dielectric constant $\varepsilon_1(0)$ was 5.63. The calculated linear absorption spectrum is shown in Fig.6. The absorption edge starts at about 1.8 eV and corresponds to the energy gap $\Gamma^{\mathrm{V}}$-$M^{\mathrm{C}}$. This originates from the transition from O-2$p$ electron states located at the top

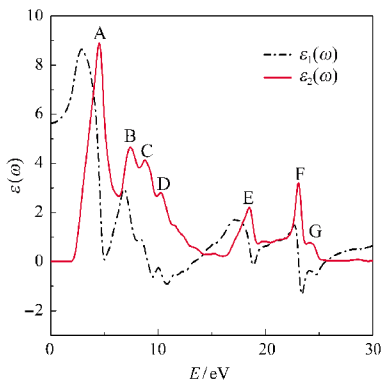


**Fig.5 Calculated real part $\varepsilon_1(\omega)$ and imaginary part $\varepsilon_2(\omega)$ of the dielectric function $\varepsilon(\omega)$ of $BaTiO_3$**

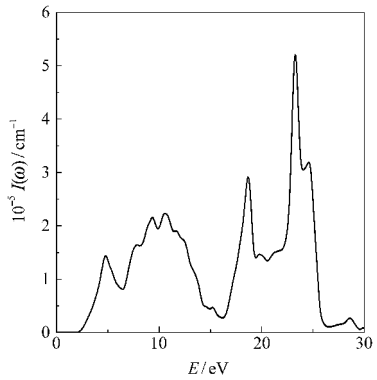


**Fig.6 Calculated absorption coefficient $I(\omega)$ of $BaTiO_3$**

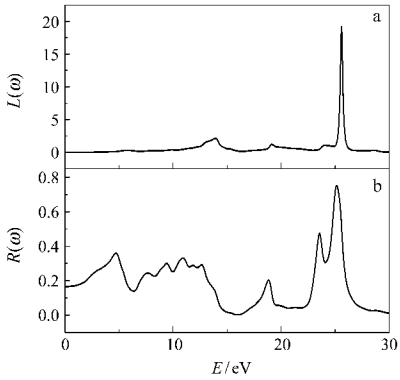


**Fig.8 Calculated electron energy loss $L(\omega)$ spectrum (a) and optical reflectivity $R(\omega)$ spectrum (b) of $BaTiO_3$**

of the valence bands to the empty Ti 3*d* electron states that dominate the bottom of the conduction bands. These also explain the origin of the peak structure in the reflectivity and the absorption coefficient spectra. The first peak in the absorption spectrum is at 4.76 eV. Other peaks are at 7.72, 9.28, 10.69, 18.71, 23.24, and 24.64 eV, respectively. According to our dielectric function calculation, the energy of each absorption peak is due to the transition of electron excitation from the VB to the CB in the electronic energy band structure. The Ba atom contributes almost nothing to the low-energy part of the linear absorption spectrum. This is because its electronic states are not in the domain of major interest. The refractive index provides useful information about the optical properties of the material. The extinction coefficient directly describes the attenuation of electromagnetic waves within the material and is also known as a damping constant or attenuation coefficient. The refractive index and the extinction coefficient are given in Fig.7. The static refractive index $n(0)$ is found to have a value of 2.36. This value increases with increasing the energy in the transparency region and reaches a peak in the ultraviolet at about 3.10 eV. It then decreases to a minimum at 25.21 eV. The local maxima of the extinction coefficient $k(\omega)$ corresponds to the zero of $\varepsilon_1(\omega)$. The origin of the structures in the imaginary part of the dielectric function also explains the structures in the refractive index. The

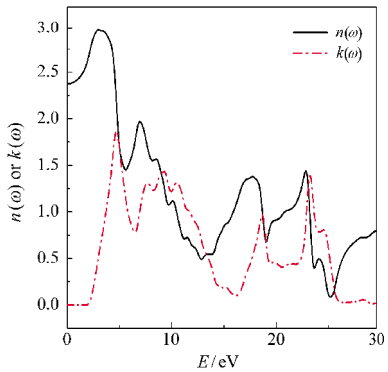


**Fig.7 Calculated refractive index $n(\omega)$ and extinction coefficient $k(\omega)$ of $BaTiO_3$**

electron energy loss function $L(\omega)$ is an important factor describing the energy loss of a fast electron traversing in a material. Prominent peaks in $L(\omega)$ spectra represent the characteristics associated with the plasma oscillations and the corresponding frequencies are the so-called bulk plasma frequency $\omega(p)$, which occurs where $\varepsilon_2<1$ and $\varepsilon_1$ reaches the zero point[27]. Moreover, the main peak of $L(\omega)$ (Fig.8a) at about 25.58 eV corresponds to an abrupt reduction of $R(\omega)$ (Fig.8b), which is better than the values of 5 and 25 eV calculated by TB-LMTO[9] and FLAPW-SAT[12], respectively. From the earlier description, our calculated optical constants of the dielectric function, absorption spectrum, refractive index, extinction coefficient, reflectivity, and energy loss coefficient are in good agreement with experimental data[14] in a wide-energy ranges.

## 3 Conclusions

The electronic structures of cubic and tetragonal $BaTiO_3$ and optical properties of cubic $BaTiO_3$ were studied in detail. Calculations show that there is a typical underestimate of lattice parameters in the LDA and that the GGA approximation gives lattice parameters closer to experimental values. An indirect band gap of 2.02 eV in the $\Gamma$-$M$ direction for the cubic phase and an indirect band gap of 2.20 eV in the $\Gamma$-$X$ direction for the tetragonal phase are calculated. Although hybridization is present between Ti-3*d* and O-2*p* orbitals, the calculations of Mulliken charge population reveal that the overlapping electron distribution on shorter Ti—O bonds in tetragonal $BaTiO_3$ is smaller than that for Pb—O bonds in tetragonal $PbTiO_3$ and this predicts a difference in ferroelectric behavior between $PbTiO_3$ and $BaTiO_3$. The dielectric function, absorption spectrum, refractive index, extinction coefficient, reflectivity, and energy loss coefficient are also in good agreement with experimental data in the low- and high-energy regions. Using the band structure, the interband contribution to optical response functions was analyzed. Predictions show that O-2*p* states and Ti-3*d* states play a major role in these optical transitions as initial and final states, respectively. Our predictions offer information that is essential for a better understanding of ferroelectric properties and for the design of novel materials based on orbital physics.

## References


1 Cohen, R. E. *Nature*, **1992, 358**: 136

2 Cohen, R. E.; Krakauer, H. *Phys. Rev. B*, **1990, 42**: 6416

3 Zhong, W.; Vanderbilt, D. *Phys. Rev. Lett.*, **1994, 73**: 1861

4 Paul, J.; Nishimatsu, T. *Indian Acad. Sci.*, **2008, 70**: 263

5 Piskunov, S.; Heifets, E.; Eglitis, R. I.; Borstel, G. *Comput. Mater. Sci.*, **2004, 29**: 165

6 Chen, X. S.; Lu, W.; Shen, S. C. *Solid State Commun.*, **2004, 130**: 641

7 Salehi, H.; Hosseini, S. M.; Shahtahmasebi, N. *Ceram. Int.*, **2004, 30**: 81

8 Wample, S. H.; Didomenico, M.; Camlibel, I. J. *Phys. Chem. Solids*, **1968, 29**: 1797

9 Saha, S.; Sinha, T. P. *Phys. Rev. B*, **2000, 62**: 8828

10 Ahuja, R.; Eriksson, O.; Johansson, B. *J. Appl. Phys.*, **2001, 90**: 1854

11 Spitzer, W. G.; Miller, R. C.; Kleinman, D. A.; Howed, L. E. *Phys. Rev.*, **1962, 126**: 1710

12 Cai, M. Q.; Yin, Z.; Zhang, M. S. *Appl. Phys. Lett.*, **2003, 83**: 2805

13 Kuroiw, Y.; Aoyagi, S.; Sawada, A. *Phys. Rev. Lett.*, **2001, 87**: 217601

14 Bäuerle, D.; Braun, E.; Saile, V.; Sppussel, G.; Kock, E. E. *Z. Phys. B*, **1978, 29**: 179

15 Payne, M. C.; Teter, M. P.; Allan, D. C.; Arias, T. A.; Joannopoulos, J. D. *Rev. Mod. Phys.*, **1992, 64**: 1045

16 Segall, M. D.; Lindan, P. J. D.; Probert, M. J.; Pickard, C. J.; Hasnip, P. J.; Clark, S. J.; Payne, M. C. *J. Phys. Condens. Matter*, **2002, 14**: 2717

17 Ghosez, P.; Desquesnes, D.; Gonze, X.; Rabe, K. M. *AIP Conf. Proc.*, **2000, 535**: 102

18 Monkhorst, H. J.; Pack, J. D. *Phys. Rev. B*, **1976, 13**: 5188

19 Ambrosch-Draxl, C.; Sofo, J. O. *Comput. Phys. Commun.*, **2006, 175**: 1

20 Samantaray, C. B.; Sim, H.; Hwang, H. *Appl. Surf. Sci.*, **2005, 250**: 146

21 Hellwege, K. H.; Hellwege, A. M.; Landolt-Börnstein. Berlin: Springer Berlin Heidelberg Press, 1969: 88–104

22 Freire, J. D.; Katiyar, R. S. *Phys. Rev. B*, **1988, 37**: 2074

23 Khenata, R.; Sahnoun, M.; Baltache, H.; Rérat, M.; Rashek, A. H.; Illes, N.; Bouhafs, B. *Solid State Commun.*, **2005, 136**: 120

24 Palomino-Rojas, L. A.; López-Fuentes, M. *Solid State Sci.*, **2008, 10**: 1228

25 Wang, Y. X.; Zhong, W. L.; Wang, C. L.; Zhang, P. L. *Solid State Commun.*, **2001, 102**: 133

26 Sun, J.; Zhou, X. F.; Fan, Y. X.; Chen, J.; Wang, H. T. *Phys. Rev. B*, **2006, 73**: 045108

27 De Almeida, J. S.; Ahuja, R. *Phys. Rev. B*, **2006, 73**: 165102